

Quantum Light from Lossy Semiconductor Rydberg Excitons

Valentin Walther^{1,2,*} and Anders S. Sørensen³

¹*ITAMP, Harvard-Smithsonian Center for Astrophysics, Cambridge, Massachusetts 02138, USA*

²*Department of Physics, Harvard University, Cambridge, Massachusetts 02138, USA*

³*Center for Hybrid Quantum Networks (Hy-Q), The Niels Bohr Institute, University of Copenhagen, DK-2100 Copenhagen Ø, Denmark*

 (Received 16 November 2022; accepted 28 June 2023; published 21 July 2023)

The emergence of photonic quantum correlations is typically associated with emitters strongly coupled to a photonic mode. Here, we show that semiconductor Rydberg excitons, which are only weakly coupled to a free-space light mode can produce strongly antibunched fields, i.e., quantum light. This effect is fueled by a micron-scale excitation blockade between Rydberg excitons inducing pair-wise polariton scattering events. Photons incident on an exciton resonance are scattered into blue- and red-detuned pairs, which enjoy relative protection from absorption and thus dominate the transmitted light. We demonstrate that this effect persists in the presence of additional phonon coupling, strong nonradiative decay, and across a wide range of experimental parameters. Our results pave the way for the observation of quantum statistics from weakly coupled semiconductor excitons.

DOI: 10.1103/PhysRevLett.131.033607

Semiconductor excitons, bound electron-hole pairs, have been at the forefront of semiconductor research ever since their discovery in the 1950s. One of their central features is their optical activity [1] and hence their innate ability to interface with light. These capabilities have been demonstrated in a number of observations including polariton formation [2], parametric scattering [3,4], four-wave mixing [5,6], optical bistability [7,8] and polariton lasing [9,10]. Despite intense recent efforts [11,12], pushing these effects down to the level of individual photons has proven difficult. The observation of highly excited Rydberg states of excitons [13] promises access to strong interactions [14], an ingredient that may prove valuable for producing quantum light using the effect of Rydberg blockade, as pioneered in atomic gases with great success [15–17].

In Rydberg blockade, the presence of an excitation inside the medium inhibits the excitation of another Rydberg state within the so-called blockade radius R_b , which in semiconductors can be several microns large [18]. The highest principal quantum number of $n \sim 30$ and largest associated blockade radii were observed in the so-called yellow series of Cu_2O [13,19,20]. These exciton states feature only relatively weak dipole transition elements, as the valence and conduction band have the same parity [21]. In addition, the exciton series is superimposed by a phonon-assisted absorptive background, which can account for more than half of the absorption on a Rydberg exciton resonance [Fig. 1(a)]. While both factors, in general, counteract the buildup of quantum correlations, we here describe conditions under which quantum light can still be observed from lossy semiconductor Rydberg excitons.

In particular, we describe the transmission of light through a crystal with Rydberg excitons, e.g., Cu_2O , and show that the transmitted light can develop quantum properties. Importantly, these correlations survive even in the presence of strong damping, a regime typically incompatible with elusive quantum effects. As such, the resulting dynamics may open up a new regime in the exploration of excitons, and may provide insights into the parameters of

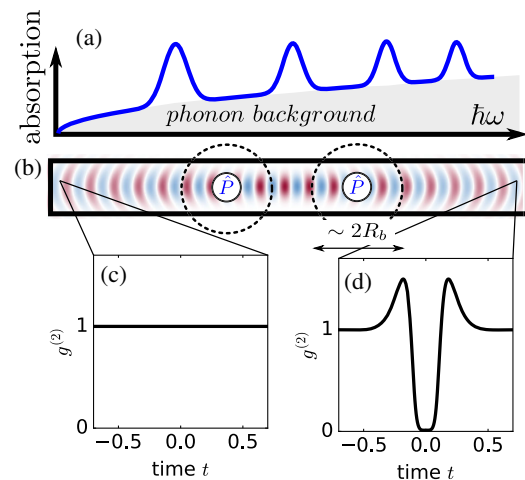


FIG. 1. The spectrum of Rydberg excitons, as in cuprous oxide, is often superimposed on a broad phonon-assisted absorptive background (a). Rydberg excitons (\hat{P}), as created by near-resonant light, blockade each other over a distance of R_b (b). This correlated dynamics converts a weak coherent beam at the input (c) into a highly nonclassical photonic state (d), as evidenced by the second-order correlation function $g^{(2)}(0) \approx 0$ (for $L \approx 2.4$, $\beta = 10$, $R_b = 0.1$).

these system, which are currently poorly understood. We further establish a formal link between Rydberg exciton transmission and discrete scatterers coupled to waveguides [22,23]. We expect that this connection will be a fruitful link for the exploration of excitonic Rydberg states, where quantum states of light have so far not been observed.

We consider a cuprous oxide crystal of thickness L which is illuminated by a light beam detuned by $\Delta = \omega - \omega_x$ from one of the discrete exciton resonances ω_x (Fig. 1). Focusing on a paraxial light beam and a single transverse mode, the slowly varying electric-field envelope of the electromagnetic field can be described by the bosonic operator $\hat{\mathcal{E}}(\mathbf{r})$ that yields the photon density operator $\hat{\mathcal{E}}^\dagger \hat{\mathcal{E}}$. It propagates at the group velocity v_g [24] and near resonantly couples to excitons, described by the bosonic operator $\hat{\mathcal{P}}(\mathbf{r})$. However, it also couples to a broad absorptive phonon-assisted resonance that underlies the Rydberg exciton spectrum in Cu_2O [25]. This background can be integrated out [26] to effectively give a finite absorption rate γ_{bg} . The light propagation is hence described by the effective Hamiltonian

$$\begin{aligned} \hat{\mathcal{H}}_0/\hbar = & -\Delta \int d\mathbf{r} \hat{\mathcal{P}}^\dagger(\mathbf{r}) \hat{\mathcal{P}}(\mathbf{r}) + g \int d\mathbf{r} \hat{\mathcal{P}}^\dagger(\mathbf{r}) \hat{\mathcal{E}}(\mathbf{r}) + \text{H.c.} \\ & + \int d\mathbf{r} \hat{\mathcal{E}}^\dagger(\mathbf{r}) \left(-iv_g \partial_z + \frac{\hbar}{2m_\perp} \nabla_\perp^2 \right) \hat{\mathcal{E}}(\mathbf{r}) \\ & - i\gamma_{\text{bg}} \int d\mathbf{r} \hat{\mathcal{E}}^\dagger(\mathbf{r}) \hat{\mathcal{E}}(\mathbf{r}), \end{aligned} \quad (1)$$

with the light-matter coupling strength g and the transverse effective mass $m_\perp = \hbar n \omega_x / (c v_g)$ with the dielectric constant n and the speed of light c . The source of photon correlations lies in the extraordinarily strong interactions between highly excited Rydberg excitons [27], giving rise to an excitation blockade wherever they exceed the exciton linewidth γ . While the optically active excitons in Cu_2O have p -state character and are thus multiply degenerate [28,29], we employ here a simplified model with a single effective potential energy surface [30] $\hat{\mathcal{V}} = \frac{1}{2} \int d\mathbf{r} \int d\mathbf{r}' V(|\mathbf{r} - \mathbf{r}'|) \hat{\mathcal{P}}^\dagger(\mathbf{r}) \hat{\mathcal{P}}^\dagger(\mathbf{r}') \hat{\mathcal{P}}(\mathbf{r}') \hat{\mathcal{P}}(\mathbf{r})$ with $V(R) = C_6/R^6$. The total Hamiltonian is thus $\hat{\mathcal{H}} = \hat{\mathcal{H}}_0 + \hat{\mathcal{V}}$.

The quantum dynamics in the semiconductor are described by expanding the wave function into sectors with different excitation numbers. When the crystal is excited by a weak coherent light field, higher excitation sectors are suppressed by a small amplitude α . Therefore, we approximate the full state using sectors with 0, 1, and 2 excitations. In the single-excitation sector, the excitation can reside in either the photon or the exciton: $|\Psi(t)\rangle^{(1)} = \int d\mathbf{r} E(\mathbf{r}, t) \hat{\mathcal{E}}^\dagger(\mathbf{r}) |\emptyset\rangle + \int d\mathbf{r} P(\mathbf{r}, t) \hat{\mathcal{P}}^\dagger(\mathbf{r}) |\emptyset\rangle$. In the doubly excited sector, the possible combinations

are having two photons $[EE(\mathbf{r}, \mathbf{r}', t)]$, two excitons $[PP(\mathbf{r}, \mathbf{r}', t)]$ or one of each $[EP(\mathbf{r}, \mathbf{r}', t)]$, where the first coordinate describes the photon and the second the exciton location.

To elucidate the system dynamics, we apply the Schrödinger equation to each excitation sector $|\Psi(t)\rangle^{(n)}$. Loss from the n -excitation sector can, in principle, contribute to the sectors with fewer excitations. However, due to the relative suppression with α such contributions are small and can be neglected, leaving separate dynamics in each sector. The noninteracting paraxial wave equations are solved by the complete set of Laguerre-Gauss and Hermite-Gauss modes. For simplicity, we project into the lowest such mode, the TEM_{00} mode, and discuss the general case in Ref. [31].

The equations of motion for a single excitation are

$$\partial_t E(z, t) = -v_g \partial_z E(z, t) - \gamma_{\text{bg}} E(z, t) - igP(z, t), \quad (2)$$

$$\partial_t P(z, t) = -igE(z, t) - \frac{\Gamma}{2} P(z, t), \quad (3)$$

where we have defined the complex linewidth $\Gamma = \gamma - 2i\Delta$ with γ being the combined excitonic decay (out of the mode) and dephasing rate. We consider continuous wave (cw) driving such that for times long compared to the relaxation time $1/\gamma$, the system will be in the steady state ($\partial_t E = 0$, $\partial_t P = 0$) and we obtain

$$P(z) = -\frac{2ig}{\Gamma} E(z), \quad E(z) = \alpha e^{-\left(\frac{2\gamma^2}{v_g^2} + \frac{\gamma_{\text{bg}}}{v_g}\right)z}, \quad (4)$$

describing standard Beer-Lambert absorption. This solution reveals some important quantities, which we employ to rescale our equations: the resonant excitonic field absorption length, $l_{\text{abs}} = (v_g \gamma / 2g^2)$ ($z \rightarrow z/l_{\text{abs}}$), the associated absorption time, $t_{\text{abs}} = l_{\text{abs}}/v_g$ ($t \rightarrow t/t_{\text{abs}}$), the ratio of coherence and absorption lengths, $\beta = \gamma^2/(4g^2)$, and the scaled detuning $\delta = \Delta/\gamma$. We thus denote all distances in units of l_{abs} , all times in units of t_{abs} and all energies in units of \hbar/t_{abs} . To focus on the effects of interactions, we move to an interaction picture by factoring the linear solutions $f_0(z, z')$ out of each two-excitation wave function component $F(z, z')$ via $F(z, z') = f(z, z') f_0(z, z')$. As shown explicitly in Ref. [31], two excitations in the crystal then follow the coupled dynamics

$$\begin{aligned} \partial_R ee(R, r) &= \frac{2}{1 - 2i\delta} ee(R, r) - \frac{1}{1 - 2i\delta} ep_+(R, r), \\ \partial_R ep_+(R, r) &= -2\partial_r ep_-(R, r) + 4(1 - 2i\delta)\beta ee(R, r) \\ &\quad + 2(-(1 - 2i\delta)\beta - iV_{\text{eff}}(r))ep_+(R, r), \\ \partial_R ep_-(R, r) &= -2\partial_r ep_+(R, r) - 2(1 - 2i\delta)\beta ep_-(R, r) \\ &\quad + \frac{2}{1 - 2i\delta} ep_-(R, r). \end{aligned} \quad (5)$$

Here, we have switched to center-of-mass and relative coordinates, defined by $R = [(z + z')/2]$ and $r = z - z'$ and use symmetrized, ep_+ , and antisymmetrized, ep_- , wave functions. Note that these equations are only strictly valid in the cw limit, where the wave function component describing two excitons, PP , can be eliminated exactly. The general time-dependent equations are given in Ref. [31]. Special attention must be attributed to the boundary conditions of Eq. (5), describing the state of the system when one excitation is the medium, while the other has not entered or has already exited. They are given by $ee(R, r) = 1$, $ep_+(R, r) = 2$, and $ep_-(R, r) = 0$ when $z = 0$ or $z' = 0$. Conveniently, the transformations yield a particularly simple form of the second-order photonic correlation function in transmission $g^{(2)}(\tau) = |ee(L, L - v_g\tau)|^2$.

Remarkably, we observe in Eq. (5) that the problematic phonon-assisted absorption background γ_{bg} has been identically eliminated from the equations via the ansatz in Eq. (4) [31], showing that the photon correlations in transmission are immune to loss from such parallel absorption pathways. Thus, we can analyze the transmission of an initially flat beam through the Cu_2O crystal (as illustrated in Fig. 1) and interpret the emergent correlations as signatures of the semiconductor's Rydberg excitations.

A key role is played by the effective potential V_{eff} , which breaks the noninteracting solution and induces correlations. As derived in Ref. [31], its functional form is

$$V_{\text{eff}}(r) = -\frac{1}{2\delta + i} + \frac{1}{2\delta - \frac{R_b^6}{r^6} + i}. \quad (6)$$

Figure 2(a) illustrates the effective potential for resonant excitation and repulsive exciton-exciton interactions [32]. Its dominant feature is a short-ranged nonperturbative plateau of width R_b that represents a nonlinear reduction of absorption, corresponding to a gain in the rescaled variables. In addition, there is a ‘‘refractive’’ effect at finite distances, reflecting a change in the effective detuning caused by a Rydberg excitation.

Strictly speaking, the photon propagation defines a boundary value problem on the domain $(z, z') \in [0, L]$. However, since the absorption length in Cu_2O is much longer than the blockade radius, $l_{\text{abs}} \gg R_{\text{bl}}$, the minimal build-up of correlations when the photons enter and exit the crystal can be neglected and Eq. (5) be solved as an initial value problem, as shown in Ref. [31].

We begin discussing the case of long coherence length ($\beta \approx 1$), where an excitation has equal coupling rate to the input mode and other channels. Figure 2(b) shows how propagation through the crystal converts an initially flat state into a nontrivial photonic correlation function: After short propagation distances, the $g^{(2)}$ function develops a dip at short time separations τ , which subsequently widens and deepens, until it hits the limit of very antibunched light,

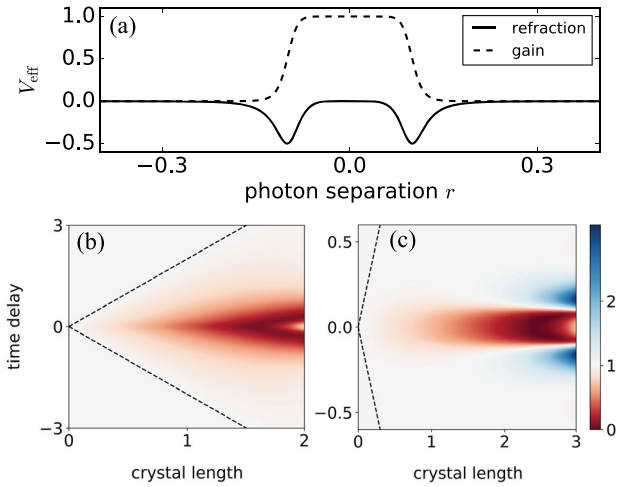


FIG. 2. During their propagation through the crystal, the excitations are subject to a Rydberg-mediated interaction potential (a), featuring nonlinear absorption or gain (imaginary part, dashed line) as well nonlinear refraction (real part, solid line). The response at short distances takes a flat-top profile, reflecting the excitation blockade, shown here for $R_b = 0.1$. Low-loss conditions (b) ($\beta = 1$) feature long-range photon correlations, and photon bunching at $t = 0$ for long crystals, while high-loss (c) ($\beta = 10$) evokes correlations on the scale of R_b and finite-time bunching for long crystals. In either case, quantum light, $g^{(2)}(0) < 0$, can be found at some crystal lengths. Dashed lines mark the crystal boundaries.

$g^{(2)}(0) \approx 0$. Beyond that point, the second-order correlation function grows and develops a distinct maximum at $\tau = 0$, while new minima emerge at finite τ . In the limit of very long crystals, we find bunched light $g^{(2)}(0) \rightarrow \infty$.

The above behavior can be understood by unraveling the scattering events in the crystal. Transforming Eq. (5) into reciprocal space in the relative coordinate yields $i\partial_R \vec{\psi}(R) = (\mathbf{H}_0 + \mathbf{V})\vec{\psi}(R)$, with a noninteracting diagonal matrix \mathbf{H}_0 and an off-diagonal interaction matrix \mathbf{V} . This offers a convenient perturbation expansion in \mathbf{V} , i.e., in the number of scattering events. We obtain $\vec{\psi}(L) = \mathbf{T}(L)\vec{\psi}(0)$ with the transfer matrix $\mathbf{T}(L) = \exp(-i[\mathbf{H}_0 + \mathbf{V}]L) = \mathbf{T}^{(0)}(L) + \mathbf{T}^{(1)}(L) + \dots$. The lowest orders are $\mathbf{T}^{(0)}(L) = \exp(-i\mathbf{H}_0L)$ and

$$\mathbf{T}^{(1)}(L) = -i \int_0^L \exp(-i\mathbf{H}_0 R) \mathbf{V} \exp[-i\mathbf{H}_0(L - R)] dR. \quad (7)$$

This perturbation expansion can easily be implemented by discretizing the integral, mapping it to the dynamics of light interacting with discrete scatterers, such as atoms coupled to a waveguide [33,34].

The first-order approximation to the scattering is excellent and reproduces the exact numerical results very well. The observed second-order photonic correlations functions [Fig. 2(b)] thus find a simple interpretation: \mathbf{V} projects the first-order scattered waves into the state ep_+ , which then

pick up a phase shift π upon emission, and add up coherently during the propagation [22]. They then interfere with the uncorrelated zeroth-order wave, which is an eigenstate of \mathbf{H}_0 , resulting in destructive interference and the observed antibunched light feature in $g^{(2)}$. With increasing propagation distance, the amplitude of the first-order wave components at $\tau = 0$ cancels the zeroth order weight and gives the special point $g^{(2)}(0) \approx 0$. We note that this cancellation is not perfect as the scattered wave amplitudes carry an imaginary component. Beyond the point of minimal $g^{(2)}(0)$, the same scattered wave functions dominate and ultimately lead to the bunching feature in $g^{(2)}(0)$.

If the loss rate is large ($\beta \gg 1$), qualitatively different photon correlations emerge in transmission, cf. Figs. 1 and 2(c). In this case, the photonic correlation function also develops a dip after short propagation distances but its features are much narrower, limited now by the blockade radius R_b . This can be explained by a single excitation blocking the creation of another exciton. A second photon will thus move faster until it eventually slows down again when it is a blockade radius away. Furthermore, the depression in $g^{(2)}$ still continues to the critical point of $g^2(0) \approx 0$ but additionally forms wings at finite time delay τ , shortly before $g^{(2)}(0)$ begins growing again. The resulting photon correlations for reasonably long crystals still feature a significant reduction from the classical limit of $g^{(2)}(0) \geq 1$, indicating the quantum nature of the transmitted light. For even larger β , the minimal value of $g^{(2)}(0)$ grows and the mentioned wings followed by finite-time bunching develop earlier. For very long crystals, the bunching feature at *finite* τ dominates the correlations.

A convenient picture for the lossy regime is given by the complex eigenstates of \mathbf{H}_0 , the ‘‘polariton basis’’ [Figs. 3(a)–3(b)]. While the dispersion relations are almost independent of the loss rate β , the damping rate of two polariton branches is proportional to β . For large β , these branches thus do not appreciably contribute to the dynamics and we can formulate an effective description in terms of the remaining polariton branch, $\vec{\phi}(R)$, alone: $i\partial_R \vec{\phi}(R) = \omega(k)\vec{\phi}(R) + \tilde{\mathbf{V}}\vec{\phi}(R)$, with the complex polariton branch $\omega(k)$ and the projected interaction matrix $\tilde{\mathbf{V}}$. Much like in the above case of low absorption, a scattering event induces a phase shift, leading to interference with the unperturbed wave component and, ultimately, the reduction of $g^{(2)}(0) < 1$. Figure 3(c) shows this evolution of a single complex partial scattered polariton wave, $\phi^{(1)}$, propagating through the crystal after the scattering event. Conserving overall momentum, the interaction spreads the initial polariton wave from $k = 0$ into a range of relative momenta [Fig. 3(d)]. The scattered polariton pairs thus contain a red- and a blueshifted polariton each, which are both detuned from the exciton resonance and thus enjoy relative protection from absorption. These frequency components, whose characteristic length scale is given by the inverse

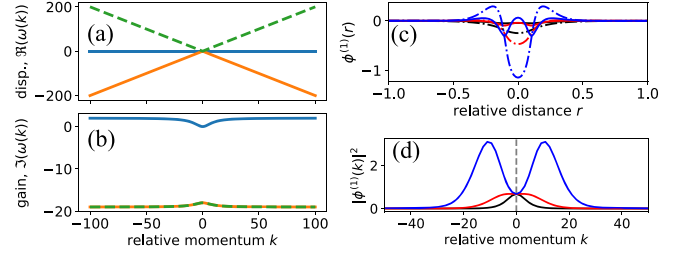


FIG. 3. For large loss ($\beta = 10$), the three polariton branches have quasilinear dispersion relations (a). Two of the branches are strongly damped, leaving a single active polariton (b). After a scattering event, the polariton wave’s imaginary component (dashed dotted) develops a pronounced dip at $r = 0$, while the real component (solid) plays a minor role, as illustrated for propagation distances $\Delta R = 0$ (black), $\Delta R = 1$ (red), and $\Delta R = 2$ (blue) at $R_b = 0.1$ (c). In momentum space, the emergence of finite-time wings can be understood from the dominance of off-resonant wave components that are relatively protected from absorption (d). Color coding as in (c).

blockade radius R_b^{-1} , hence experience relative gain, and eventually dominate the transmitted wave. The competition between interference and momentum-dependent damping results in the initial dip in $g^{(2)}(0)$ shown in Fig. 2(c), followed by the dominance of photon pairs with finite separations $\tau \sim R_b$ after long propagation lengths.

Photonic correlations are particularly interesting when they cannot originate from a classical state of light, as evidenced by the criterion $g^{(2)}(0) < 1$ [35,36]. It is, therefore, an important question under which conditions ‘‘quantum light’’ can be produced by Rydberg excitons under the influence of loss. Figure 4 shows a map of $g^{(2)}(0)$ as a function of the loss β and the crystal length L for resonant excitation conditions. We observe that for given β there is an optimal range of crystal lengths making the photonic state most nonclassical. Lower values of β are, in general, helpful for the emergence of quantum light. Remarkably, nonclassical light can, however, even be found under very

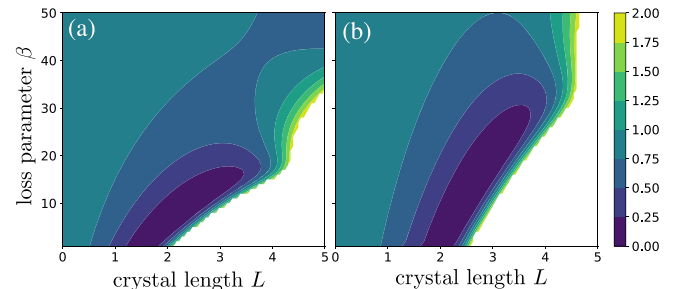


FIG. 4. The second-order correlation function at zero time delay, $g^{(2)}(0) < 1$, indicates quantum light for a wide range of parameters at corresponding optimal crystal lengths L . The blockade radii are $R_b = 0.1$ and $R_b = 0.05$ in (a) and (b), respectively. All values $g^{(2)}(0) > 2$ are whitened out for better visibility.

large loss, $\beta \gg 1$. Smaller blockade radii can enhance the light's quantum features, although the required crystal lengths tend to be longer. This phenomenon can be traced back to the wider spread of momentum states that are populated by the scattering interaction, which are better protected from absorption.

In conclusion, we have demonstrated that quantum light can be expected from the propagation of weak coherent light through a semiconductor crystal under a wide span of parameters. The excitonic field absorption lengths of cuprous oxide Rydberg states range from tens to hundreds of microns, depending on the addressed principal quantum number n [13]. The blockade radii have been measured to be several microns, justifying the assumed ratios $R_b/l_{\text{abs}} \lesssim 10\%$. Remarkably, the presence of a parallel absorption pathway, as given by a phonon-assisted background, is insignificant for the photon correlations in transmission, although it will increase the time required to measure the predicted correlations [37]. Nonradiative decay, on the other hand, has a strong bearing and tends to suppress quantum states of light. To the best of our knowledge, the value of β has not been determined experimentally. However, even for dissipation ratios as large as $\beta = 40$, quantum light can be obtained. These photonic correlations can be seen as unambiguous signatures of the Rydberg states and be used to benchmark their interactions. Furthermore, this Letter formalizes the link between atom-coupled waveguides and Rydberg photonics and shows that the easily controllable crystal length takes the place of the difficult-to-control number of atoms at the waveguide, the main cause of imperfect antibunching [22].

The underlying mechanism in the present Letter is the modulation of absorption. Exciting outlooks therefore include using loss-mitigating schemes, that correlate photons through dynamical changes in the dispersion. The simplest such example is the dispersive limit ($\Delta > \gamma$), as discussed in Ref. [31]. There, the dynamics becomes fully coherent and can be described by an effective Schrödinger equation for the correlated motion of the photon pair through the crystal with an effective mass and a photon potential. Other promising avenues to explore are electromagnetically induced transparency [26] and cavity polaritons [11,12,38]. Under such conditions, it could be possible to observe more exotic effects, such as photon bound states [39–42], Efimov states [43], and many-body states [44–46] including photon trains [47–49] and topological states [50,51].

We thank Björn Schriniski and Yuxiang Zhang for helpful discussions. V. W. thanks the Niels Bohr Institute for its hospitality for two visits, during which most of the work was completed. This work was supported by the NSF through a grant for the Institute for Theoretical Atomic, Molecular, and Optical Physics at Harvard University and the Smithsonian Astrophysical Observatory. A. S. acknowledges the support

of Danmarks Grundforskningsfond (DNRF 139, Hy-Q Center for Hybrid Quantum Systems).

*vwalther@purdue.edu

- [1] E. F. Gross, *Nuovo Cimento* (1955–1965) **3**, 672 (1956).
- [2] C. Weisbuch, M. Nishioka, A. Ishikawa, and Y. Arakawa, *Phys. Rev. Lett.* **69**, 3314 (1992).
- [3] P. G. Savvidis, J. J. Baumberg, R. M. Stevenson, M. S. Skolnick, D. M. Whittaker, and J. S. Roberts, *Phys. Rev. Lett.* **84**, 1547 (2000).
- [4] P. G. Savvidis, J. J. Baumberg, R. M. Stevenson, M. S. Skolnick, D. M. Whittaker, and J. S. Roberts, *Phys. Rev. B* **62**, R13278 (2000).
- [5] C. Ciuti, P. Schwendimann, B. Deveaud, and A. Quattropani, *Phys. Rev. B* **62**, R4825 (2000).
- [6] C. Ciuti, P. Schwendimann, and A. Quattropani, *Phys. Rev. B* **63**, 041303(R) (2001).
- [7] A. Baas, J. P. Karr, H. Eleuch, and E. Giacobino, *Phys. Rev. A* **69**, 023809 (2004).
- [8] A. Amo, T. C. H. Liew, C. Adrados, R. Houdré, E. Giacobino, A. V. Kavokin, and A. Bramati, *Nat. Photonics* **4**, 361 (2010).
- [9] S. Kim, B. Zhang, Z. Wang, J. Fischer, S. Brodbeck, M. Kamp, C. Schneider, S. Höfling, and H. Deng, *Phys. Rev. X* **6**, 011026 (2016).
- [10] D. Bajoni, *J. Phys. D* **45**, 313001 (2012).
- [11] G. Muñoz-Matutano, A. Wood, M. Johnsson, X. Vidal, B. Q. Baragiola, A. Reinhard, A. Lemaître, J. Bloch, A. Amo, G. Nogues, B. Besga, M. Richard, and T. Volz, *Nat. Mater.* **18**, 213 (2019).
- [12] A. Delteil, T. Fink, A. Schade, S. Höfling, C. Schneider, and A. Imamoglu, *Nat. Mater.* **18**, 219 (2019).
- [13] T. Kazimierczuk, D. Fröhlich, S. Scheel, H. Stolz, and M. Bayer, *Nature (London)* **514**, 343 (2014).
- [14] V. Walther, S. O. Krüger, S. Scheel, and T. Pohl, *Phys. Rev. B* **98**, 165201 (2018).
- [15] T. Peyronel, O. Firstenberg, Q.-Y. Liang, S. Hofferberth, A. V. Gorshkov, T. Pohl, M. D. Lukin, and V. Vuletic, *Nature (London)* **488**, 57 (2012).
- [16] M. Saffman and T. G. Walker, *Phys. Rev. A* **66**, 065403 (2002).
- [17] Y. O. Dudin and A. Kuzmich, *Science* **336**, 887 (2012).
- [18] V. Walther and T. Pohl, *Phys. Rev. Lett.* **125**, 097401 (2020).
- [19] S. Steinhauer, M. A. M. Versteegh, S. Gyger, A. W. Elshaari, B. Kunert, A. Mysyrowicz, and V. Zwiller, *Commun. Mater.* **1**, 11 (2020).
- [20] M. A. M. Versteegh, S. Steinhauer, J. Bajo, T. Lettner, A. Soro, A. Romanova, S. Gyger, L. Schweickert, A. Mysyrowicz, and V. Zwiller, *Phys. Rev. B* **104**, 245206 (2021).
- [21] R. J. Elliott, *Phys. Rev.* **108**, 1384 (1957).
- [22] A. S. Prasad, J. Hinney, S. Mahmoodian, K. Hammerer, S. Rind, P. Schneeweiss, A. S. Sørensen, J. Volz, and A. Rauschenbeutel, *Nat. Photonics* **14**, 719 (2020).
- [23] S. Mahmoodian, M. Čepulkovskis, S. Das, P. Lodahl, K. Hammerer, and A. S. Sørensen, *Phys. Rev. Lett.* **121**, 143601 (2018).
- [24] M. O. Scully and M. S. Zubairy, *Quantum Optics* (Cambridge University Press, Cambridge, England, 1997).

- [25] F. Schöne, H. Stolz, and N. Naka, *Phys. Rev. B* **96**, 115207 (2017).
- [26] V. Walther, P. Grünwald, and T. Pohl, *Phys. Rev. Lett.* **125**, 173601 (2020).
- [27] M. Saffman, T. G. Walker, and K. Mølmer, *Rev. Mod. Phys.* **82**, 2313 (2010).
- [28] R. J. Elliott, *Phys. Rev.* **124**, 340 (1961).
- [29] F. Schöne, S.-O. Krüger, P. Grünwald, H. Stolz, S. Scheel, M. Aßmann, J. Heckötter, J. Thewes, D. Fröhlich, and M. Bayer, *Phys. Rev. B* **93**, 075203 (2016).
- [30] J. Stanojevic, P. Grangier, and R. Côté, *J. Phys. B* **49**, 124003 (2016).
- [31] See Supplemental Material at <http://link.aps.org/supplemental/10.1103/PhysRevLett.131.033607> for details on the derivation of the model, the mode expansion of finite beams and the dispersive limit.
- [32] J. B. Balewski, A. T. Krupp, A. Gaj, S. Hofferberth, R. Löw, and T. Pfau, *New J. Phys.* **16**, 063012 (2014).
- [33] D. E. Chang, J. S. Douglas, A. González-Tudela, C.-L. Hung, and H. J. Kimble, *Rev. Mod. Phys.* **90**, 031002 (2018).
- [34] J. D. Hood, A. Goban, A. Asenjo-Garcia, M. Lu, S.-P. Yu, D. E. Chang, and H. J. Kimble, *Proc. Natl. Acad. Sci. U.S.A.* **113**, 10507 (2016).
- [35] D. F. Walls and G. J. Milburn, *Quantum Optics* (Springer Science & Business Media, New York, 2007).
- [36] J. R. Chavez-Mackay, P. Grünwald, and B. M. Rodríguez-Lara, *Phys. Rev. A* **101**, 053815 (2020).
- [37] K. Kusmierek, S. Mahmoodian, M. Cordier, J. Hinney, A. Rauschenbeutel, M. Schemmer, P. Schneeweiss, J. Volz, and K. Hammerer, [arXiv:2207.10439](https://arxiv.org/abs/2207.10439).
- [38] K. Orfanakis, S. K. Rajendran, V. Walther, T. Volz, T. Pohl, and H. Ohadi, *Nat. Mater.* **21**, 767 (2022).
- [39] M. F. Maghrebi, M. J. Gullans, P. Bienias, S. Choi, I. Martin, O. Firstenberg, M. D. Lukin, H. P. Büchler, and A. V. Gorshkov, *Phys. Rev. Lett.* **115**, 123601 (2015).
- [40] S. H. Cantu, A. V. Venkatramani, W. Xu, L. Zhou, B. Jelenković, M. D. Lukin, and V. Vuletić, *Nat. Phys.* **16**, 921 (2020).
- [41] P. Bienias, S. Choi, O. Firstenberg, M. F. Maghrebi, M. Gullans, M. D. Lukin, A. V. Gorshkov, and H. P. Büchler, *Phys. Rev. A* **90**, 053804 (2014).
- [42] Q.-Y. Liang, A. V. Venkatramani, S. H. Cantu, T. L. Nicholson, M. J. Gullans, A. V. Gorshkov, J. D. Thompson, C. Chin, M. D. Lukin, and V. Vuletić, *Science* **359**, 783 (2018).
- [43] M. J. Gullans, S. Diehl, S. T. Rittenhouse, B. P. Ruzic, J. P. D’Incao, P. Julienne, A. V. Gorshkov, and J. M. Taylor, *Phys. Rev. Lett.* **119**, 233601 (2017).
- [44] P. Bienias, J. Douglas, A. Paris-Mandoki, P. Titum, I. Mirgorodskiy, C. Tresp, E. Zeuthen, M. J. Gullans, M. Manzoni, S. Hofferberth, D. Chang, and A. V. Gorshkov, *Phys. Rev. Res.* **2**, 033049 (2020).
- [45] O. A. Iversen and T. Pohl, *Phys. Rev. Lett.* **126**, 083605 (2021).
- [46] O. A. Iversen and T. Pohl, *Phys. Rev. Res.* **4**, 023002 (2022).
- [47] T. Pohl, E. Demler, and M. D. Lukin, *Phys. Rev. Lett.* **104**, 043002 (2010).
- [48] M. Moos, M. Höning, R. Unanyan, and M. Fleischhauer, *Phys. Rev. A* **92**, 053846 (2015).
- [49] J. Otterbach, M. Moos, D. Muth, and M. Fleischhauer, *Phys. Rev. Lett.* **111**, 113001 (2013).
- [50] L. W. Clark, N. Schine, C. Baum, N. Jia, and J. Simon, *Nature (London)* **582**, 41 (2020).
- [51] R. O. Umucalılar, J. Simon, and I. Carusotto, *Phys. Rev. A* **104**, 023704 (2021).